Structure of hepatitis B/D antiviral drug Bulevirtide bound to its receptor protein NTCP

Hongtao Liu[1], Dariusz Zakrzewicz[2], Kamil Nosol[1], Rossitza N. Irobalieva[1], Somnath Mukherjee[4], Rose Bang-Sørensen[1], Nora Goldmann[3], Sebastian Kunz[2], Lorenzo Rossi[1], Anthony A. Kossiakoff[4,*], Stephan Urban[5,6,*], Dieter Glebe[3,*], Joachim Geyer[2,*], & Kaspar P. Locher[1,*]

[1]Institute of Molecular Biology and Biophysics, ETH Zürich, Zürich, Switzerland

[2]Institute of Pharmacology and Toxicology, Faculty of Veterinary Medicine, Justus Liebig University Giessen, Giessen, Germany

[3]Institute of Medical Virology, National Reference Centre for Hepatitis B Viruses and Hepatitis D Viruses, German Center for Infection Research (DZIF, Partner Site Giessen-Marburg-Langen), Justus Liebig University Giessen, Giessen, Germany

[4]Department of Biochemistry and Molecular Biology, The University of Chicago, Chicago, IL, USA

[5]Department of Infectious Diseases, Molecular Virology, University Hospital Heidelberg, Heidelberg, Germany

[6]German Center for Infection Research (DZIF) - Heidelberg Partner Site, Heidelberg, Germany

*To whom correspondence may be addressed. Email: Stephan.Urban@med.uni-heidelberg.de, koss@bsd.uchicago.edu, Dieter.Glebe@viro.med.uni-giessen.de, Joachim.M.Geyer@vetmed.uni-giessen.de, locher@mol.biol.ethz.ch

Abstract

Cellular entry of the hepatitis B and D viruses (HBV/HDV) require binding of the viral surface polypeptide preS1 to the hepatobiliary transporter NTCP. This interaction can be blocked by bulevirtide (BLV, formerly Myrcludex B), a preS1 derivative and approved drug for treating HDV infection. To elucidate the basis of this inhibitory function, we determined a cryo-EM structure of BLV-bound human NTCP. BLV forms two domains, a plug lodged in the bile salt transport tunnel of NTCP and a string that covers the receptor's extracellular surface. The N-terminally attached myristoyl group of BLV interacts with the lipid-exposed surface of NTCP. Our structure reveals how BLV inhibits bile salt transport, rationalizes NTCP mutations that decrease the risk of HBV/HDV infection, and provides a basis for understanding the host specificity of HBV/HDV. Our results provide opportunities for structure-guided development of inhibitors that target HBV/HDV docking to NTCP.

Introduction

With approximately 1.5 million individuals infected annually, the hepatitis B virus (HBV) continues to pose a substantial global health challenge, despite the availability of an effective vaccine[1]. HBV, a small, enveloped DNA virus, causes acute and chronic infection of the liver and the chronic form, in particular, significantly contributes to the overall burden of liver-related diseases, such as cirrhosis and hepatocellular carcinoma (HCC)[2,3]. Additionally, co-infection of HBV-infected patients with the hepatitis D virus (HDV), an enveloped RNA satellite virus that uses HBV surface proteins in HBV/HDV co-infected cells for envelopment and infection, enhances the severity of liver disease[4-6]. Since HBV and HDV share the HBV surface proteins to target hepatocytes for infection, their entry mechanisms have been studied extensively[7,8]. Viral entry involves initial low-affinity binding to cellular heparan sulfate proteoglycans (HSPGs)[9-12] followed by high-affinity binding to the human Na^+-taurocholate co-transporting polypeptide (NTCP), an interaction crucial for HBV/HDV infection (Fig. 1)[8,13,14]. NTCP (SLC10A1), a member of the solute carrier transporter family, is one of four transporters involved in the enterohepatic circulation of bile salts[15-17]. Located in the basolateral membrane of hepatocytes, NTCP plays a vital role in transporting approximately 80% of bile salts, particularly conjugated bile salts, from the bloodstream into hepatocytes[18,19]. Its function is linked to maintaining bile salt homeostasis, essential for the digestion and absorption of dietary fats[18]. In 2012, NTCP was identified as a receptor for HBV/HDV[8,13,14]. In 2022, four independent studies reported structures of NTCP, revealing nine transmembrane helices (TMs) arranged in two domains, termed panel and core[20-23]. Two of these helices create a crossing motif (X-motif), near which two sodium ion binding sites are located[23]. The highest-resolution structure revealed the binding sites for two bile salt molecules in a continuous tunnel that links the extracellular and cytoplasmic side of the basolateral membrane[23].

The viral envelopes of HBV and HDV contain three surface proteins: large (LHBs), middle (MHBs), and small (SHBs), generated from a single open reading frame through

alternative start codons[24-26]. They contain the same C-terminus but differ by N-terminal additions and N-glycosylation status. The SHBs contain four transmembrane domains that are embedded in the viral membrane and are linked by intra- and intermolecular disulfide bridges. The MHBs only contain a preS2-domain, whereas the LHBs contain a preS2- and a preS1-domain located N-terminal to the SHBs[27]. During protein synthesis, the LHBs undergo a posttranslational modification via myristoylation at a conserved glycine residue (Gly2) in the preS1-domain[24,28,29]. Previous studies have shown that the first 75 residues of preS1 are important for viral infectivity of HBV/HDV[30,31]. Residues ^{9}NPLGFFP^{15} are essential for infectivity and binding and are highly conserved within the ten known genotypes of HBV (GtA-GtJ)[32]. Previous studies suggest that residues Gly2-Asp48 bind to NTCP[32]. Specific regions of NTCP, including extracellular loop 1 that connects TM2 and TM3 (residues Arg84-Asn87), and the extracellular surface of TM5 (residues Lys157-Leu165), have been shown to interact with the preS1 peptide[8,14,33]. The exact mechanism of NTCP-mediated virus entry remains elusive; however, it is thought to occur via endocytosis, which is known to recruit various host factors for entry initiation[34,35]. During active HBV infections, two distinct species of viral particles are produced: infectious virus particles and a far larger excess of non-infectious subviral particles (SVPs)[36-38]. Whilst both species contain all three viral envelope proteins, allowing for recognition and binding to NTCP as a receptor, SVPs lack genetic material and are therefore not infectious[38,39]. Thus, SVPs provide an alternative model system for the study of HBV/HDV receptor interaction.

It was recognized that strategies aimed at inhibiting or disrupting binding of preS1 to NTCP hold promise in preventing HBV/HDV infection. In 2023, the commercially available drug Hepcludex® (also known as bulevirtide (BLV), formerly Myrcludex B), received market approval for the treatment of chronic HDV infection in Europe[32,40-43]. The sequence of BLV is derived from that of preS1 from HBV genotype C (residues Gly2-Gly48) with a shortening of the 11 additional N-terminal amino acids and one amino acid substitution, Gln46Lys[32]. BLV exhibits a remarkably high inhibitory constant (IC_{50} = 140 pM) against HBV and HDV in primary

human hepatocytes and HepaRG cells[32,44]. BLV has also been demonstrated to inhibit the NTCP-mediated uptake of bile salts, but at an IC_{50} in the nanomolar range[45].

We here report a cryo-electron microscopy (cryo-EM) structure of BLV-bound human NTCP, simultaneously providing insight into the mechanism of BLV inhibition and into the interaction between NTCP and the viral preS1 peptide. Coupled with functional analysis, our study advances the molecular understanding of how BLV blocks HBV/HDV infection. These findings hold promise for developing additional therapeutic interventions against HBV/HDV, preventing viral entry into hepatocytes, and thus reducing HBV/HDV-related liver damage. Furthermore, our data may help rationalize why HBV infectivity is affected by variations in NTCP among different species.

Results and Discussion

Interaction of bile salts, preS1, and patient-derived SVPs with NTCP

NTCP was previously demonstrate to transport bile salts in a strictly sodium-dependent manner[46]. We observed that a fluorescently labeled taurocholate derivative (NBD-TC) is taken up into NTCP-expressing HEK293 cells in a sodium-dependent manner (Fig. 2a). Transport of NBD-TC can only be detected by using a transport buffer containing 143 mM NaCl, while NBD-TC fluorescence is undetectable in sodium-free buffer (equimolar substitution of NaCl with choline chloride). In contrast, the fluorescently labeled preS1 derivative preS1-AX568 binds to NTCP-expressing HEK293 cells under both sodium-containing and sodium-free conditions, indicating that preS1-binding to NTCP does not require sodium (Fig. 2b). Binding of preS1-AX568 to NTCP can be blocked by preincubation with 250 µM taurocholic acid (TC) (Fig. 2a, b), confirming previous data in NTCP-expressing HepG2 hepatoma cells[13]. We then analyzed if preparations of HBV SVPs obtained from patients chronically infected with HBV are capable to bind recombinantly expressed NTCP protein as used for structure determination in the present study. HBV SVPs contain all surface proteins, namely SHBs, MHBs, and the preS1-bearing LHBs that are also enveloping the HBV/HDV virus particles (Fig.

2c). The SVP preparations represent the HBV genotypes D (GtD, patient ID1) and A (GtA, patient K826) (Fig. 2d). In both preparations the preS1-containing LHBs can be clearly detected by silver-stained polyacrylamide gel electrophoresis, although patient K826 showed a more prominent signal than patient ID1 (Fig. 2d). Plates were then coated with these patient-derived SVPs and binding of nanodisc-reconstituted, YFP-labeled NTCP[23] was observed by fluorescence measurement. We found a concentration-dependent binding of NTCP (25-100 nM) to GtA and GtD SVPs, demonstrating binding of NTCP to the SVPs. As a control, we used a NTCP variant carrying the mutation G158R, which abolished binding to the SVPs (Fig. 2e, 2f).

Functional analysis and BLV on TC transport

Bile salt transport in NTCP-expressing HEK293 cells was also analyzed with the radiolabeled bile acid ^{3}H-TC that showed robust uptake into the cells in the presence of media containing sodium (Fig. 3a). TC transport was inhibited at increasing concentrations of BLV with an inhibition constant value (IC_{50}) of 195 nM (95% CI, 174-218 nM) (Fig. 3a). At high concentrations, BLV fully abolished transport. This is consistent with the previously shown result for myristoylated preS1 inhibition of TC uptake into NTCP-expressing HEK293 cells (IC_{50} of 190 nM)[13,47], indicating that our NTCP construct is functional and suitable for further studies on interaction with BLV.

Isolation of a Fab specific to the NTCP-BLV complex

Several antibody fragments specific to human NTCP were previously reported[20-23]. The preS1 peptide is known to interact with the extracellular surface of NTCP[8,14]. All binders reported in the literature bind to the same region[20-23], suggesting an overlap in binding epitopes and therefore, incompatibility with preS1 and BLV. Hence, to gain structural insight into how BLV interacts with NTCP we aimed to generate an antigen-binding antibody fragment (Fab) specific to the NTCP-BLV complex. We generated a complex of detergent-solubilized, biotinylated NTCP and BLV (Supplementary Fig. 1a), which was used as a target for isolating Fabs from

synthetic library E[48] using phage display (Supplementary Fig. 1b). During each round of the selection, a molar excess of the BLV peptide was maintained to ensure saturation of the binding epitope. We identified one Fab, termed Fab3, that formed a stable complex with NTCP in the presence of BLV, with an apparent K_d value of 8 nM (Supplementary Fig. 2). We found that Fab3 could form a complex with NTCP in the absence of BLV (Supplementary Fig. 1c), suggesting that Fab3 specifically recognizes the NTCP-BLV complex.

Cryo-EM structure of human NTCP bound to BLV

For structural studies, we formed a complex of NTCP (38 kDa), BLV, Fab3 (50 kDa) and a Fab-binding nanobody[49] (Nb, 15 kDa), and used a monodisperse fraction of the complex for single particle cryo-EM analysis (Fig. 3b). We obtained a 3.4 Å EM density map revealing excellent density for NTCP, bound BLV, and Fab3. The structure of NTCP was similar to that of the previously reported, substrate-bound NTCP[23], featuring a translocation tunnel in an open conformation (Fig. 3c and Supplementary Fig. 3). The EM map revealed well-resolved density for BLV located both in the tunnel and on the surface of NTCP, allowing us to build all 47 amino acids and the myristoyl moiety of the BLV peptide (Supplementary Fig. 4). Consistent with our biochemical analysis, Fab3 is bound on the extracellular surface and interacts with the C-terminus residues of BLV and four regions of NTCP (N-terminus, ECL1, ECL2, and ECL4) (Fig. 3c).

BLV interactions with NTCP and Fab3

BLV has a large interface with NTCP, with 2064 $Å^2$ buried surface area between them, rationalizing the tight binding of BLV (and by extension preS1) to its receptor. Based on the structural observations, we divided the sequence of the BLV peptide into three sections - the myristoyl group, the “plug” (residues Gly2-Asp20), and the “string” (residues Pro21-Gly48) (Fig. 4a, b). Note that for consistency, residue numbering of BLV follows that of the preS1 domain of LHBs of genotype D (HBV GtD) (Fig. 4c). The myristoyl group of BLV interacts with the surface of TM4 (Phe128, Leu131, and Met133) and TM5 (Tyr156) of NTCP and is exposed to

lipids from the outer leaflet of the basolateral hepatocyte membrane. Lipidation has been identified as a crucial factor in stabilizing the binding of viral peptides[32], and a previous study demonstrated a significant decrease in viral peptide binding in the absence of myristoylation[32]. Absence of N-terminal myristoylation of preS1 by experimental mutation of Gly2 did not lead to abrogation of viral assembly and release but rendered HBV non-infectious[50,51]. Furthermore, during the development of BLV, peptides that did not contain a myristoyl moiety exhibited low or negligible antiviral activity[32]. The location of the myristoyl group places the first amino acid, Gly2, at the external entrance of the NTCP tunnel (Fig. 4a, d). Interestingly, for most HBV genotypes (besides genotypes D and J), the preS1 peptide contains up to an additional 11 residues between the myristylation motif and Gly2 of the plug domain (Fig. 4c). Our structure suggests that these residues are not involved in receptor recognition as they are most likely exposed to the cell exterior and would not disturb the interaction of the plug and string domains of preS1 with NTCP.

Starting with Gly2, the first 19 residues of BLV adopt a globular shape that forms a plug wedged inside the translocation tunnel and reaching the middle of the membrane bilayer (Fig. 4d, e). It was previously shown that deleting the plug region from inhibitory myr-preS1 peptides (HBVpreS/19-48^{myr}) abrogates their inhibitory potential on HBV infection[28,40]. In addition, deletion within the preS1 plug region of LHBs abolishes the infectivity of HBV[31]. Notably, residues Gly2-Asp20 are highly conserved (Fig. 4c). Only three of the plug residues, Thr3, Val7, and Pro8, differ among the preS1 genotypes: Thr3 is exposed to the solvent, whereas Val7 and Pro8 are replaced in the preS1 genotypes D, E and G by ones of a similar size, such as threonine, serine or alanine. Furthermore, several conserved residues of the BLV peptide (Leu11-Phe14) contain hydrophobic side chains exposed toward the lumen of the translocation tunnel (Fig. 4e). Among these, Phe14 is replaced by a leucine residue only in the preS1 of genotypes G and I. When the mutation is introduced in genotype C (as in BLV), it does not affect the ability of the virus to bind to hepatocytes[8].

The string domain of BLV (Pro21-Gly48) cover the surface of the plug (Fig. 4f) and cross the extracellular surface of NTCP (Fig. 4g). The importance of the string domain of preS1 for viral infectivity was previously established[31]. Deletions in the string domain in infection-interfering myr-preS1 peptides (Δ20-21, Δ20-23, Δ23-27) reduce, but do not abolish the inhibitory activity of those peptides in competition assays with HBV[28]. Several side chains of the string domain are exposed to the solvent (Asn28, Asn29, Asp31, Asn37, Glu43, Asn45, Lys46) and do not interact with NTCP (Fig. 4c), which rationalizes why some of these are poorly conserved within preS1 among different genotypes. The C-terminus of the string (Glu42-Gly48) binds to ECL1 of NTCP, a region that contains the sequence ^{84}RLKN^{87} reported to be essential for host discrimination specificity[8,14,33]. This region is variable in different mammalian species. In mice, the corresponding residues are ^{84}HLTS^{87}, and it was observed that mice hepatocytes can bind human HBV/HDV, but cannot be infected. However, transgenic mice containing a humanized fragment of residues 84-87 in NTCP can be infected[14,33,52]. While our structure can rationalize why mouse NTCP can bind preS1 of human HBV, it does not offer a direct reason why infectivity is unable to proceed, which is likely due to downstream events.

Binding of BLV to NTCP prevents bile salt transport

We superimposed the NTCP-BLV structure with our previously reported, substrate-bound NTCP structure containing two molecules of glycochenodeoxycholic acid (GCDC, PDB 7ZYI). While the overall root-mean-square deviation (RMSD) was only 0.767 Å, the structural differences were unevenly distributed (Fig. 5). While the core domains of the two structures are virtually identical, the helices TM1, TM5, TM6 forming the panel domain are shifted, which is likely a consequence of BLV binding. The superposition shows that the plug of the BLV peptide partly overlaps with the substrate binding pocket. Simultaneous binding is therefore impossible because it would result in a steric clash (Fig. 5). Residues Leu11 and Phe13 of BLV overlap with the scaffold of GCDC, indicating that these side chains would prevent the binding of even the shortest bile acids (Fig. 5b). Our structure therefore rationalizes why BLV

(and by extension preS1) binding to NTCP is incompatible with the binding and transport of bile salts. For patients administered BLV, an increase in bile salt levels in the plasma was observed. However, a recent clinical study showed that this increase is not significant enough to cause cholestatic liver injury or hepatocyte dysfunction[53].

In our previously reported structure of substrate-bound NTCP, we identified two sodium binding sites in the vicinity of the X-motif (Supplementary Fig. 5)[23]. However, in the BLV-bound NTCP structure, there is no density for sodium ions and the residues that have previously been shown to coordinate the binding of sodium ions, such as Glu257 and Gln261, are poorly resolved. This observation suggests that the presence of the BLV peptide prevents sodium ions from binding at high affinity, which is in line with the experimental evidence that the preS1 peptide can bind NTCP also in the absence of sodium (Fig. 2a, b), whereas bile salt transport requires sodium (Fig. 2a).

Structural implications for HBV infectivity

Given the similarity between BLV and preS1, our structure can explain the difference between variants of NTCP among species and their effect on HBV infectivity. We aligned the sequence of human NTCP to that of Cynomolgus monkey and Common squirrel monkey, which are representatives of the Old and New World monkeys, respectively (Fig. 6a and Supplementary Fig. 6). Old World monkeys are not susceptible to HBV infection due to the large side chain of arginine at position 158 of NTCP[54]. Mutation of this Arg158 into Gly158, which is conserved in human, apes and most of the New World monkey NTCPs, renders the Old World Monkey susceptible to human HBV in vitro[54]. Vice versa, Gly158Arg mutation of human and Common squirrel monkey NTCPs completely abrogates preS1 binding and HBV infection in the cell culture model, while maintaining the transport activity of NTCP for TC[54]. Our structure shows that Gly158 is located at the NTCP tunnel entrance, where it tightly packs against main chain atoms of the plug domain of BLV (Fig. 6b). As a result, any amino acid other than glycine at this position, and in particular a bulky amino acid such as arginine, will cause a steric clash

with the plug of BLV (and by extension preS1), thereby preventing binding and HBV entry and infection (Fig. 6b). This is consistent with previous studies that showed that substitution of Gly158 interferes with preS1 binding[54-56].

Another noteworthy NTCP site is the nonsynonymous human genetic variant S267F (c.800C>T) of NTCP, which is found in East Asia populations[57]. The S267F variant cannot efficiently transport bile salts[58], which is in line with the position of Ser267 near the bile acid binding sites of NTCP[23,57]. In addition, the S267F mutation reduces HBV entry and infection in cell culture experiments and has been associated with resistance to chronic HBV infection and decelerated progression of related liver diseases[59,60]. Our structure visualizes the proximity of Ser267 to the plug region of the BLV peptide (Fig. 6c), where a phenylalanine would cause a steric clash both with preS1 peptides, BLV and bile salts, which is in agreement with experimental findings[22].

While preparing this manuscript for submission, a structural study of NTCP bound to a preS1 peptide was published[61]. In their study, Asami et al. generated a NTCP-preS1 specific Fab that binds to a similar epitope as Fab3 presented in our study (Supplementary Fig. 7). Both structures reveal similar conformations of NTCP (RMSD = 0.496 Å) and the same fold for BLV (our study) and preS1 of genotype B[61]. This suggests that the Fab binders developed independently did not influence the fold of the peptides and their interactions with NTCP.

Conclusion

Our study reveals the molecular basis of viral preS1 interactions with its receptor NTCP and the inhibition of this interaction by the commercial drug bulevirtide/Hepcludex® (Fig. 6d). The results also rationalize why binding of BLV affects bile salt transport by NTCP. Furthermore, our data corroborates previous biochemical results regarding which residues in the BLV sequence are critical for inhibiting viral infection. Our findings allow us to rationalize HBV/HDV specificity for human NTCP and explain why the S267F mutation in humans presents a

compromised bile salt transport with simultaneous resistance to HBV/HDV. We identified BLV residues that face the solvent and do not appear to interact with NTCP. These might be amenable for the design of smaller drugs (peptidomimetics) that improve the pharmacology of BLV in order to prevent HBV and HDV binding and infection. Our structure also provides a starting point for rational design of HBV drugs that are not based on peptide backbones and may allow oral administration.

Methods

Protein expression and purification

The full-length wild-type human NTCP gene (UniProt ID: Q14973) was generated synthetically by GeneArt (Thermo Fisher Scientific) after codon optimization for expression in HEK293 cells. All subsequent modifications of the sequence, including the introduction of point mutations, were performed using synthetic gene fragments and were confirmed via sequencing (Microsynth). NTCP was generated as a fusion construct, containing a C-terminal 3C protease cleavage site, preceded by an eYFP-rho-1D4 tag. The NTCP construct used for Fab generation contained an Avi-tag between the C-terminal end of NTCP and the 3C protease cleavage site. Stable cell lines for expression were generated using the doxycycline-inducible Flp-In T-Rex 293 system (Thermo Fisher Scientific) according to the manufacturer's guidelines.

Cells were adapted and maintained in the fresh complete Dulbecco's Modified Eagle Medium (DMEM, Gibco) supplemented with 10% fetal bovine serum (FBS, Thermo Fisher Scientific). Cells were grown at 37°C under humidified conditions with 5% CO_2. Cell expression was induced by adding doxycycline (Sigma) to a final concentration of 3 µg/mL, whereafter cells were grown for a further 60 h in DMEM supplemented with 2% FBS under the previously mentioned conditions. Cells were harvested and flash-frozen in liquid nitrogen for storage at -80°C. All purification steps were performed at 4°C or on ice, whenever possible. Frozen cell pellets were thawed and homogenized with a Douncer in working buffer (10:1 vol/wt) containing 25 mM HEPES (pH 7.5), 150 mM NaCl, 20% glycerol, supplemented with cOmplete EDTA-free protease inhibitor tablets (Roche). Lauryl maltose neopentylglycol (L-MNG, Anatrace) was added to a final concentration of 1% (wt/vol). Solubilization took place for 2 h at 4°C with gentle agitation before centrifugation at 140,000 x g for 30 minutes using a Type Ti-45 rotor (Beckmann). The supernatant was applied to Sepharose-coupled rho-1D4 antibody resin (University of British Columbia), previously equilibrated with 10 column volumes (CVs) of working buffer supplemented with 0.01% L-MNG. This mixture was incubated for 2

hours at 4°C with gentle agitation. The 1D4 resin was hereafter washed three times with 10 CVs of washing buffer containing 25 mM HEPES (pH 7.5), 150 mM NaCl, 20% glycerol, and 0.01% L-MNG to remove unbound components. Subsequently, the 1D4 resin was incubated for 2 hours with three CVs of buffer supplemented with a 1:50 (wt:wt) ratio of 3C protease to expected protein for cleavage of the C-terminal tags of the NTCP fusion protein. The elution was concentrated using a 50 kDa molecular weight cut-off centrifugal filter (Amicon) before loading onto a Superose 6 increase column 10/300 GL (Cytiva) for size exclusion chromatography. The protein concentration in detergent micelles was determined by absorbance at 280 nm using a NanoDrop 2000c spectrophotometer (Thermo Fisher Scientific).

Nanodisc reconstitution

A mix of brain polar extract lipids (Avanti Polar Lipids) and cholesterol (Avanti Polar Lipids) (4:1 wt/wt) was solubilized in 1%/0.2% DDM/CHS (wt/wt), and thereafter sonicated. The lipids were then mixed with detergent-purified NTCP and incubated at room temperature for 5 min with gentle agitation. Next, membrane scaffold protein (MSP1D1) was added to the mixture and incubated for 20 minutes at room temperature. The molar ratio of the mixture was 1:5:100 (protein:MSP1D1:lipids). Bio-Beads SM-2 (Bio-Rad) were activated with methanol, pre-equilibrated with HBS buffer (25 mM HEPES pH 7.5, 150 mM NaCl), and were added to a concentration of 0.8 g/mL to the nanodiscs mixture and incubated overnight at 4°C with gentle mixing. Bio-Beads were removed by passing through a gravity column (Bio-Rad), and the mixture was briefly spun at 4000×g at 4°C to remove excess lipids. The sample was concentrated using a 50 kDa molecular weight cut-off centrifugal filter (Amicon), followed by size exclusion chromatography run as previously described, except now in HBS buffer. Peak fractions containing nanodisc-reconstituted NTCP were collected and concentrated.

PreS1-AX568 binding to HEK-NTCP cells

Human embryonic kidney (HEK293, Thermo Fisher Scientific) cells, stably expressing the human NTCP protein, were generated as described[62] and are further referred to as HEK-

NTCP cells. Cells were maintained at 37°C, 5% CO_2, and 95% humidity in Dulbecco's modified Eagle medium (DMEM)/Ham's F12 medium (Thermo Fisher Scientific) supplemented with 10% fetal calf serum (Sigma-Aldrich), 4 mM L-glutamine (PAA), and antibiotics (100 U/mL penicillin and 100 μg/mL streptomycin, both Anprotec) and 100 μg/mL hygromycin (Carl Roth). For induction of NTCP expression, cells were incubated with 5 μg/mL doxycycline. Qualitative transport experiments were performed with the fluorescent bile acid 4-nitrobenzo-2-oxa-1,3-diazole taurocholic acid (NBD-TC) in DMEM[63] in HEK-NTCP cells. Nuclei were stained with Hoechst33342 (Thermo Fisher Scientific) and fluorescence images were analyzed on a DMI6000 B inverted fluorescent microscope (Leica). Qualitative and quantitative preS1-peptide binding was analyzed with the NH_2-terminally myristoylated and COOH-terminally AlexaFlour 568-coupled fluorescent myr-preS1$^{2-48}$ peptide (further referred to as preS1-AX568 peptide), consisting of amino acids 2-48 of the large HBV sub-genotype D3 surface protein (Biosynthesis). Briefly, HEK293 and HEK-NTCP cells were incubated with 200 nM preS1-AX568 peptide in sodium buffer (142.9 mM NaCl, 4.7 mM KCl, 1.2 mM $MgSO_4$ x $7H_2O$, 1.2 mM KH_2PO_4, 20 mM HEPES, 1.8 mM $CaCl_2$ x $2H_2O$, pH 7.4) or in sodium-free buffer (equimolar substitution of NaCl with choline chloride). Inhibitor preincubation was performed over 5 min at 37°C. Quantification of relative fluorescence was assessed at 570 nm excitation and 615 nm emission on a fluorescence microplate reader (TECAN Life Sciences).

Patient-derived SVP preparation and binding assay

Plasma samples from HBV-infected patients were used in accordance with the ethics committee of the Justus Liebig University Giessen (AZ 257/18). Subviral particles (SVPs) were isolated from plasma of two chronic HBV-infected patients by three consecutive ultracentrifugation steps according to published protocols[13]. Briefly, SVP were separated from virions using rate zonal ultracentrifugation through a sucrose density gradient. SVP-containing fractions were pooled and further purified using caesium chloride (CsCl) flotation ultracentrifugation. Pooled SVP-fractions were further purified using a second sucrose density gradient and concentrated by ultrafiltration. SVP preparations from plasma of two different

high-titer (> 10^9 HBV genomes/mL), HBeAg- and HBsAg-positive, chronic HBV-infected patients of genotype A (patient #1, K826, HBV-GtA) and genotype D (patient #2, ID1, HBV-GtD) were used for binding assays with nanodisc-associated recombinant NTCP. Aliquots of the SVP preparations were analyzed by silver-stained polyacrylamide gels and revealed 6.3% and 12.03% LHBs for the patient #2 and #1 preparations, respectively. FluoroNunc polysorb F16 black plates (Nunc Thermo Scientific) were coated with SVPs (1 μg total/well, 20 μg/mL) overnight at 4°C and afterward blocked with HBS buffer (20 mM HEPES, pH 7.4, 150 mM NaCl) supplemented with 3% (w/v) bovine serum albumin (BSA) for 1 h at 4°C under gentle shaking. After 3x washing with HBS buffer, 50 μL (25-100 nM) of recombinant wild-type or G158R mutant NTCP-eYFP nanodisc preparations were added onto the plate and incubated for 1 h at 4°C under gentle shaking. The supernatant was slowly removed, and the samples were 3x gently washed with HBS buffer. For fluorescence measurement, 100 μL HBS buffer was added to each well and the fluorescence intensity of eYFP was detected at 485 nm excitation and 535 nm emission on a fluorescence microplate reader (TECAN Life Sciences).

Transport assay into HEK cells

The uptake of radioactive taurocholate (^{3}H-TC, American Radiolabeled Chemicals) was used to determine the transport activity of NTCP. All reactions were performed in DMEM medium at 37°C. NTCP expressed in Flp-In T-Rex 293 cells was induced upon the addition of 1 μg/ml tetracycline and grown for 24 h under standard conditions. Hereafter, the cells were detached, and 150,000 cells were seeded into each well of a Poly-D-Lysine (Sigma) coated 24-well plate (Nunc, Thermo Fisher Scientific). After the cells had adhered, the media was exchanged with a pre-warmed buffer, consisting of DMEM, and where indicated, supplemented with a dilution of BLV dissolved in water, and pre-incubated for 15 min at 37°C with gentle shaking. Hereafter, the media was removed and replaced with the pre-warmed uptake buffer, consisting of DMEM supplemented with 1 μM sodium taurocholate (TC) and BLV, maintaining the same BLV concentration as for the pre-incubation. The added TC contained a mix of radiolabeled TC (^{3}H-TC) and non-labeled TC in a 1:20 ratio (mol/mol). The uptake reaction was stopped after

8 min by washing the cells thrice with ice-cold phosphate-buffered saline (PBS, Gibco). Lysis buffer containing 1 M NaOH and 2% Triton X-100 in H_2O was added, whereafter lysed cells were added to 2 mL scintillation fluid and radioactivity was measured using a scintillation counter (Perkin Elmer 2450 Microbeta2). Data were analyzed using GraphPad Prism 8.0.0 and fitted to a four-parameter logistic curve from where the IC_{50} and the 95% confidence interval were calculated. The data were normalized to the top plateau of the curve.

Enzymatic Biotinylation of NTCP

We used biotinylated NTCP for Fab selection from the synthetic Fab library E^{48}. 3C-cleaved NTCP in detergent was biotinylated via BirA-mediated biotinylation of the NTCP Avi-tag construct in the presence of 1 μM BLV, as previously described. The yield of labeling was verified by a streptavidin pull-down assay.

Phage display selection

NTCP, biotinylated through the Avi-tag was used for phage display selection. The biotinylated Avi-tagged protein was in 40 mM HEPES, pH 7.4, 150 mM NaCl, and 0.01% L-MNG. Phage display selection was performed using the phage library E^{48} following published protocols with necessary modifications[64]. 1 μM BLV peptide was used in selection to obtain Fabs binding to the BLV-bound NTCP. In the first round, 250 nM of the target was immobilized on streptavidin magnetic beads. Over the course of several rounds of selection, the protein concentration was gradually dropped to 10 nM in the last round. From the second round onwards, the bound phages were eluted using 100 mM glycine, pH 2.7. This harsh elution technique often results in the elution of non-specific and streptavidin binders. To eliminate them, the precipitated phage pool from the second round onwards was negatively selected against streptavidin beads before adding to the target. The pre-cleared phage pool was then used as an input for the selection.

411 **Single-point phage ELISA**

412 A single-point phage ELISA was used to rapidly screen the binding of the obtained Fab
413 fragments in phage format. The ELISA experiments were also performed at 4°C in the
414 presence of 1 μM BLV peptide. Colonies of E. coli XL1-Blue harboring phagemids from the
415 last round of selection were inoculated directly into 500 μL of 2 x YT broth supplemented with
416 100 μg/mL ampicillin and M13-KO7 helper phage. The cultures were grown overnight at 37°C.
417 The experimental wells in the ELISA plates were incubated with 40 nM biotinylated NTCP in
418 ELISA buffer in the presence of 1 μM BLV peptide for 20 min. Only buffer was added to the
419 control wells. Overnight culture supernatants containing Fab phage were diluted 10-fold in
420 ELISA buffer containing 1 μM BLV peptide. The diluted phage supernatants were then
421 transferred to ELISA plates that were pre-incubated with the biotinylated target and washed
422 with ELISA buffer. The ELISA plates were incubated with the phage for another 15 min and
423 then washed with ELISA buffer. The washed ELISA plates were incubated with a 1:1 mixture
424 of mouse anti-M13 monoclonal antibody (GE, 1:5,000 dilution in ELISA buffer) and
425 peroxidase-conjugated goat anti-mouse IgG (Jackson Immunoresearch, 1:5000 dilution in
426 ELISA buffer) for 30 min. The plates were again washed, developed with TMB substrate, and
427 then quenched with 1.0 M HCl, and the absorbance at 450 nm was determined. The
428 background binding of the phage was monitored by the absorbance from the control wells.

429 **Sequencing, cloning, expression, and purification of Fab fragments**

430 From phage ELISA, positive clones (selected based on a high ratio of ELISA signal of target
431 binding to background) were identified and 6 unique clones were obtained after DNA
432 sequencing. These six binders were sub-cloned in pRH2.2, an IPTG inducible vector for
433 expression of Fabs in E. coli. E. coli C43 (Pro+) cells were transformed with sequence-verified
434 clones of Fab fragments in pRH2.2[65]. The Fabs were expressed and purified according to
435 published protocols[66].

436

437 **Multipoint Protein ELISA for EC_{50} determination**

438 Multipoint ELISA was performed at 4°C to estimate the affinity of the Fabs to NTCP in the
439 presence of BLV. 40 nM of target immobilized on a neutravidin-coated ELISA plate was
440 incubated with serial dilutions of the purified Fabs for 20 min. The plates were washed, and
441 the bound NTCP-Fab complexes were incubated with a secondary HRP-conjugated Pierce
442 recombinant protein L (Thermofisher, 1:5000 dilution in ELISA buffer) for 30 min. The plates
443 were again washed, developed with TMB substrate, and quenched with 1.0 M HCl, and
444 absorbance (A_{450}) was determined. To determine the affinities, the data were fitted in a dose-
445 response sigmoidal function in GraphPad Prism, and EC_{50} values were calculated.

446 **Fab-binding nanobody expression and purification**

447 The Fab-binding nanobody[49] construct was created by fusing one N-terminal His-tag and TEV
448 protease cleavage site in a pET26b (+) vector. This plasmid was transformed into E. coli BL21
449 (DE3) cells for expression in a terrific broth (TB) medium. The cells were grown to OD_{600} of
450 0.8 at 37°C, and then induced by the addition of 1 mM IPTG and grown for 20 h at 20°C with
451 shaking. The cells were harvested and purification of the Fab-binding nanobody took place.
452 Periplasmic protein was obtained via osmotic shock by sucrose gradient. The lysate was
453 purified by Ni-NTA chromatography, and the His-tag was removed with TEV protease.

454 **Preparation of NTCP-BLV-Fab3-nanobody complex**

455 The BLV peptide was added into the concentrated detergent-purified NTCP solution in
456 detergent at a final concentration of 1 μM, followed by mixing with Fab3 and Fab-binding
457 nanobody with a molar ratio of 1:1:1.2. The mixture was incubated on ice for 1 h and then
458 purified by SEC in buffer containing 25 mM HEPES (pH 7.5), 150 mM NaCl, 20% glycerol,
459 and 0.01% L-MNG. After SEC, the NTCP-BLV-Fab3-nanobody complex was concentrated
460 with a 50 kDa molecular weight cut-off centrifugal filter to around 3.6 mg/mL for cryo-EM grid
461 preparation.

462

Cryo-EM sample preparation

For cryo-EM grids preparation, 3.5 μL of the detergent-purified NTCP-BLV-Fab3-nanobody complex sample was applied to glow-discharged Quantifoil R1.2/1.3 carbon/copper 300 mesh grids, and then the grids were plunge-frozen in a liquid ethane-propane mixture cooled by liquid nitrogen using a Vitrobot Mark IV (FEI) at 4°C and 100% humidity.

Cryo-EM data acquisition and processing

Data was collected on a Titan Krios 300 kV (TFS) equipped with a Gatan BioContinuum energy filter and a Gatan K3 detector. Data were acquired with EPU (Thermo Fisher Scientific) at a nominal magnification of 130,000x (0.648 Å/pix). The defocus ranged from -0.5 to -2.5 μm, with a total dose of 55 $e^-/Å^2$. Data acquisition statistics are presented in Supplementary Table 1 and the data processing pipeline is presented in Supplementary Figure 3.

The multi-frame movies of the NTCP-BLV-Fab3-nanobody complex were imported into CryoSPARC v4.4.0. All movies were subjected to patch motion correction and CTF estimation using Patch CTF. Several micrographs were used for initial particle selection by blob picker and initial 2D classification. The results from the 2D classification were then used to pick 1,696,776 particles from all micrographs, followed by particle extraction with a pixel size of 0.648 Å/pix. After two rounds of 2D classification, 168,595 particles were used for ab-initio reconstruction. All particles (663,583) were further subjected to heterogeneous refinement, where after each round the best class was selected for further processing. In total, five subsequent rounds of heterogeneous refinement were performed. The remaining 153,166 particles were then subjected to non-uniform refinement and local refinement, yielding a cryo-EM density map at 3.43 Å resolution. The particles were then subjected to local motion correction, 2D classification that yielded a final set of 128,700 particles, global CTF refinement, local CTF refinement, and another local refinement, yielding a final EM density map at 3.41 Å.

Model building and refinement

The final cryo-EM map was used for model building in Coot[67]. We built the model for NTCP-BLV-Fab3-nanobody complex based on the previously reported structure of substrate-bound NTCP (PDB ID: 7ZYI). The N-terminus (residues 1-10) and C-terminus (residues 312-349) of NTCP are highly flexible and were not resolved. Model refinements were performed in Phenix[68] with geometric and secondary structure restraints and validation in MolProbity[69]. The BLV peptide showed well-resolved EM density that allowed for de novo model building based on the peptide sequence. The atomic coordinates and geometrical restraint of the ligands (myristoylated glycine) were drawn and generated by ChemDraw (PerkinElmer Informatics, Inc. Version 22.2) and Phenix eLBOW.

Figure preparation

Graph preparation and statistical analysis were performed in GraphPad 9 (macOS, GraphPad Software, La Jolla California USA, www.graphpad.com) or GraphPad Prism 10 (for Windows). The figures of models and EM density maps were prepared in PyMOL (the PyMOL Molecular Graphics System, Version 2.5, Schrödinger), UCSF Chimera[70], and UCSF ChimeraX[71].

Data availability

The atomic coordinates of the NTCP-BLV-Fab3-nanobody complex model from this study have been deposited in the Protein Data Bank (PDB) under accession code 8RQF. The cryo-EM map was deposited in the Electron Microscopy Data Bank (EMDB) under accession code EMD-19440.

Acknowledgments

We thank the Scientific Center for Optical and Electron Microscopy (ScopeM) facility at ETH Zürich for support with cryo-EM data collection. This research was supported by Swiss National Science Foundation (SNSF) grants 189111 and 214834 to K.P.L.; the Deutsche Forschungsgemeinschaft (DFG) SFB 1021, project number 197785619 (project B8 to J.G.

514 and D.G.); National Institutes of Health grant GM117372 (to A.A.K.). The National Reference
515 Centre for Hepatitis B Viruses and Hepatitis D Viruses at Justus Liebig University Giessen
516 (D.G.) is supported by the German Ministry of Health via the Robert Koch Institute, Berlin,
517 Germany.

518 Author contributions

519 H.L. and K.P.L. conceived the project. H.L. expressed and purified human NTCP, processed
520 EM data, and built the atomic model with help from K.N. D.Z. and K.N. designed preS1
521 experiments. S.K. and D.Z. conducted transport assays of NTCP. R.N.I. collected and
522 processed EM data. H.L., K.N., R.N.I., and K.L. performed structural analysis. S.M. and L.R.
523 generated conformational Fabs against NTCP. A.A.K. supervised synthetic antibody
524 generation. D.Z., N.G., and S.K. conducted the SVP and preS1-AX568 binding experiments.
525 R.B.-S. designed and performed NTCP-BLV functional assays and analyzed functional data.
526 J.G. and D.G. contributed to the discussion of the data. S.U. provided the BLV peptide and
527 insight during manuscript preparation. H.L., R.N.I., R.B.-S., K.N., J.G., D.G., and K.P.L. wrote
528 the manuscript with input from the other authors.

529 Conflict of interest

530 Stephan Urban is the inventor of and holds patents on Bulevirtide.

Figures

Fig. 1

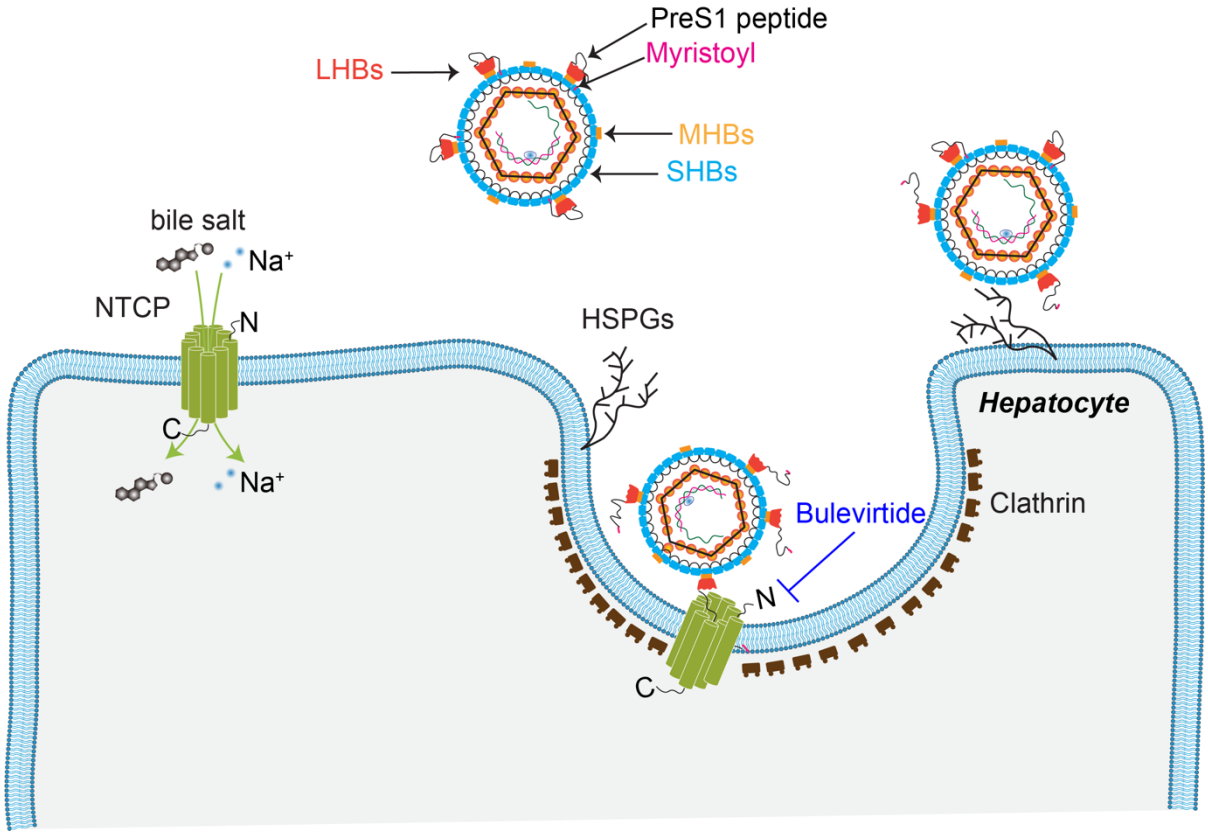

535 **Fig. 2**

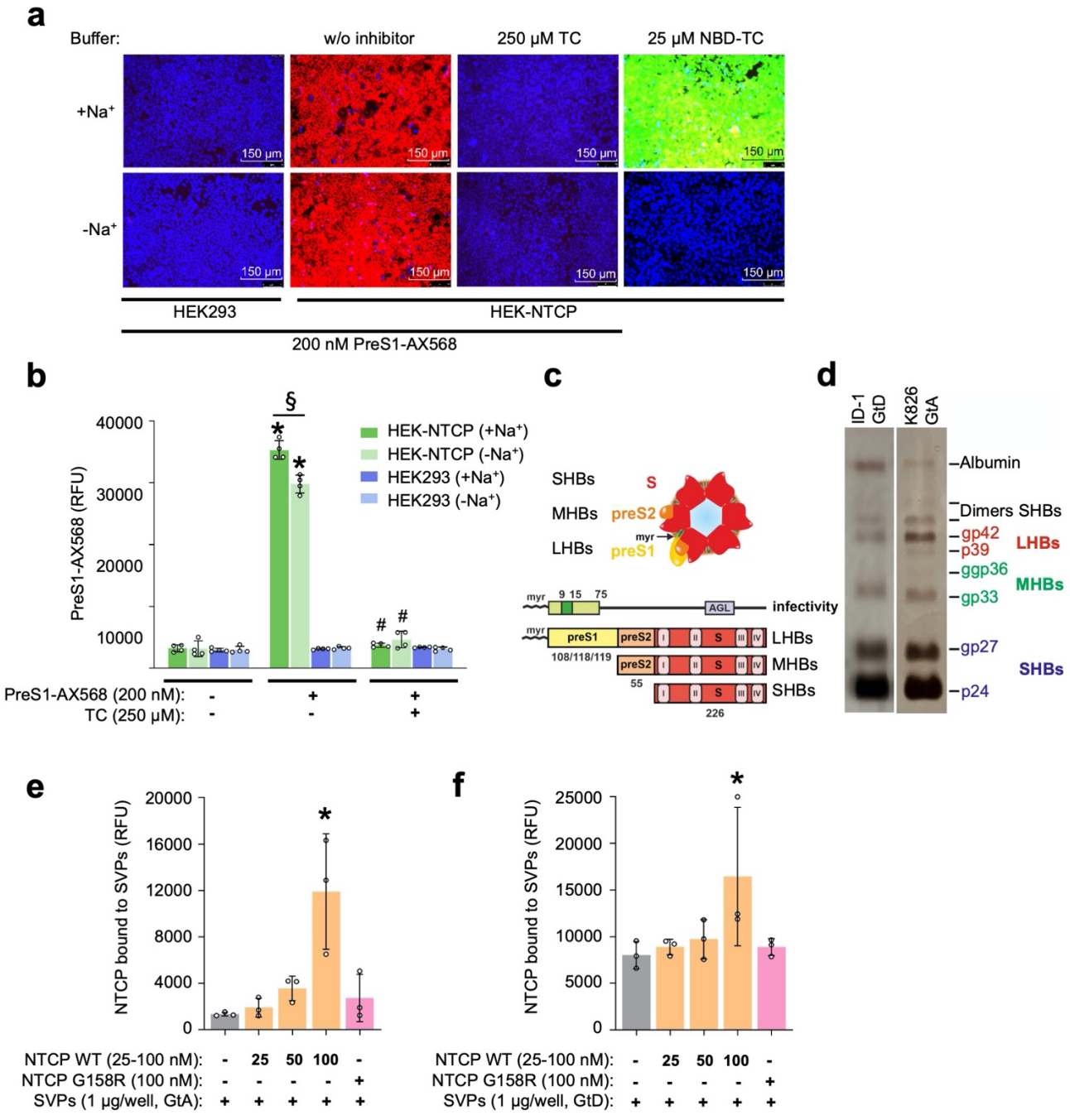

536

537

538 **Fig. 3**

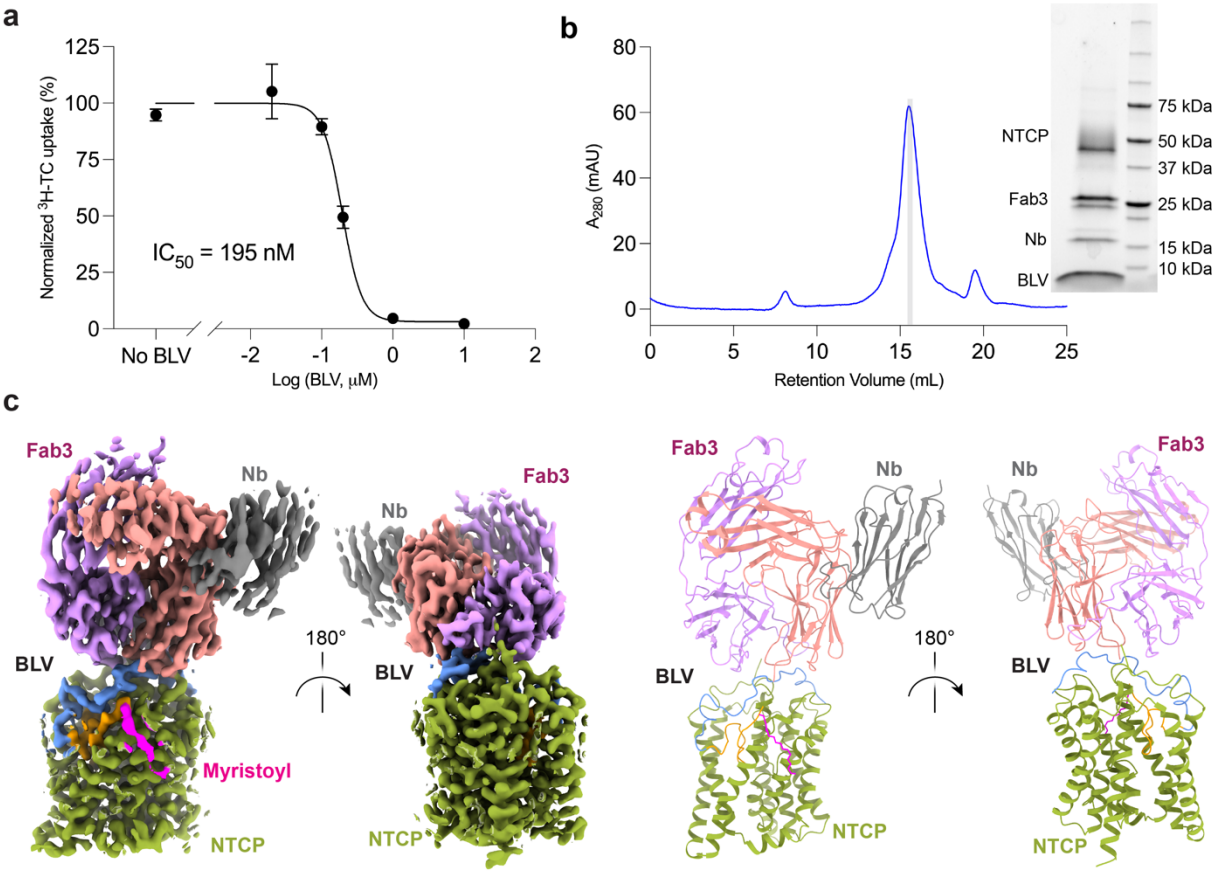

539
540

Fig. 4

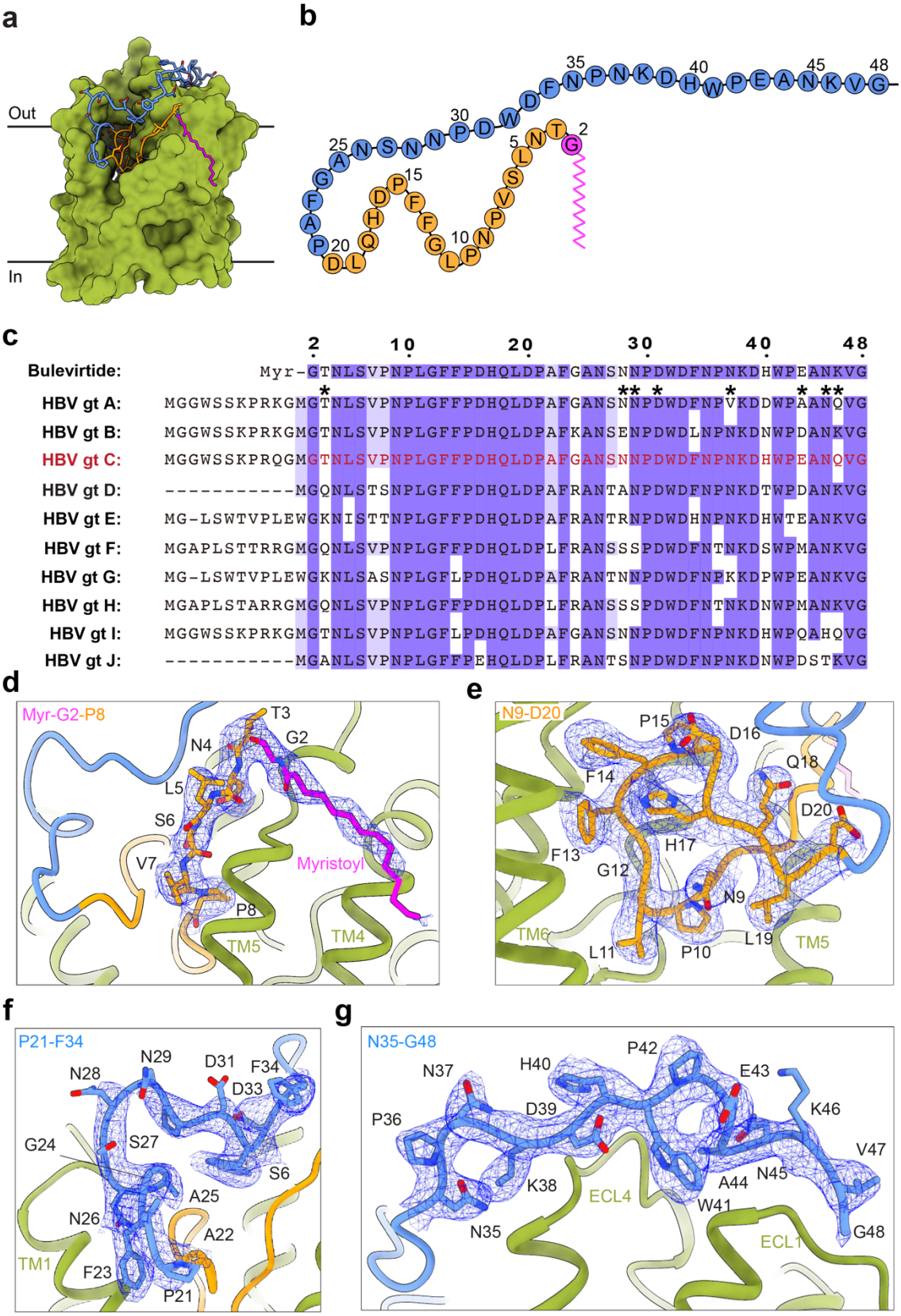

Fig. 5

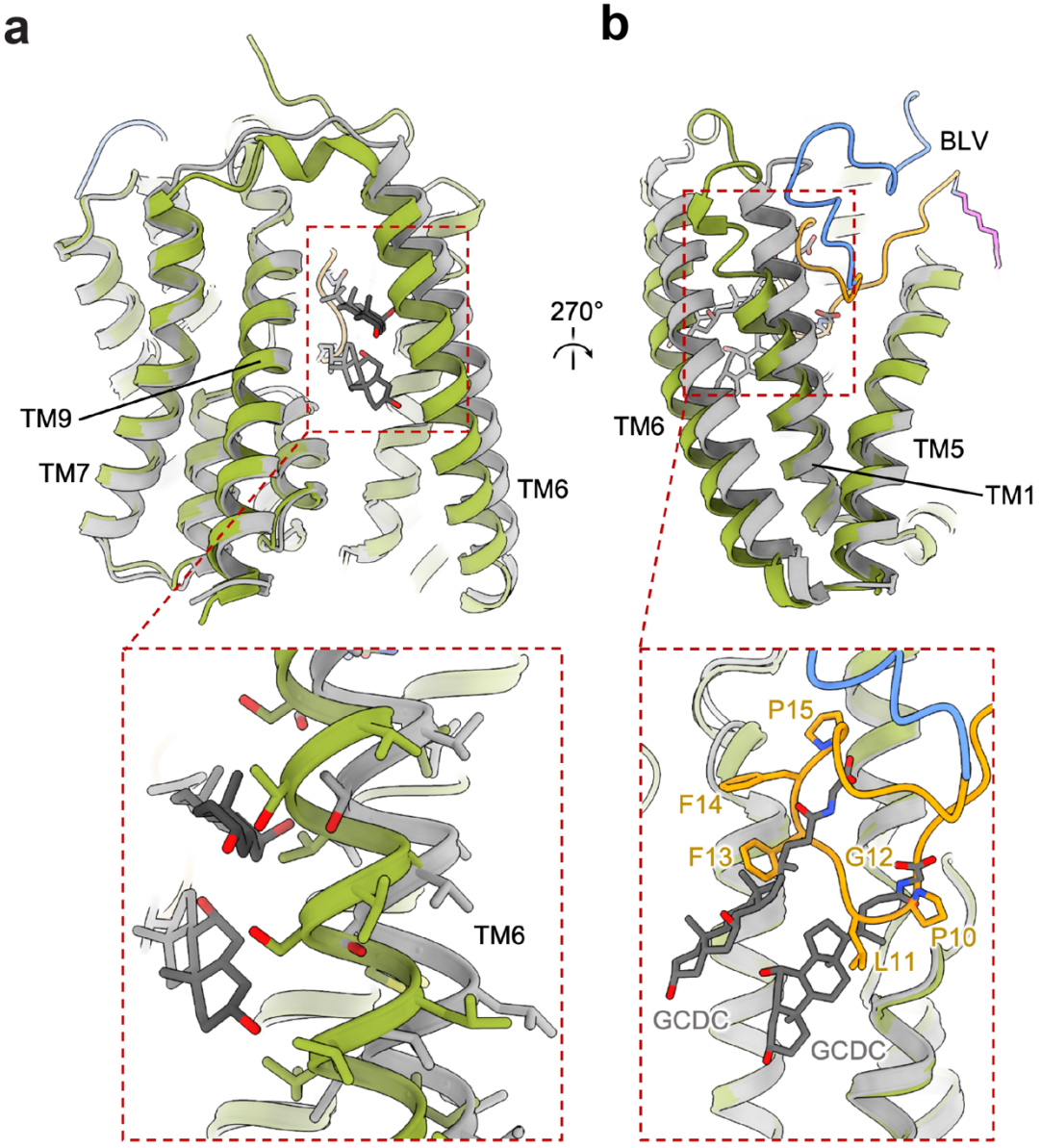

549 **Fig. 6**

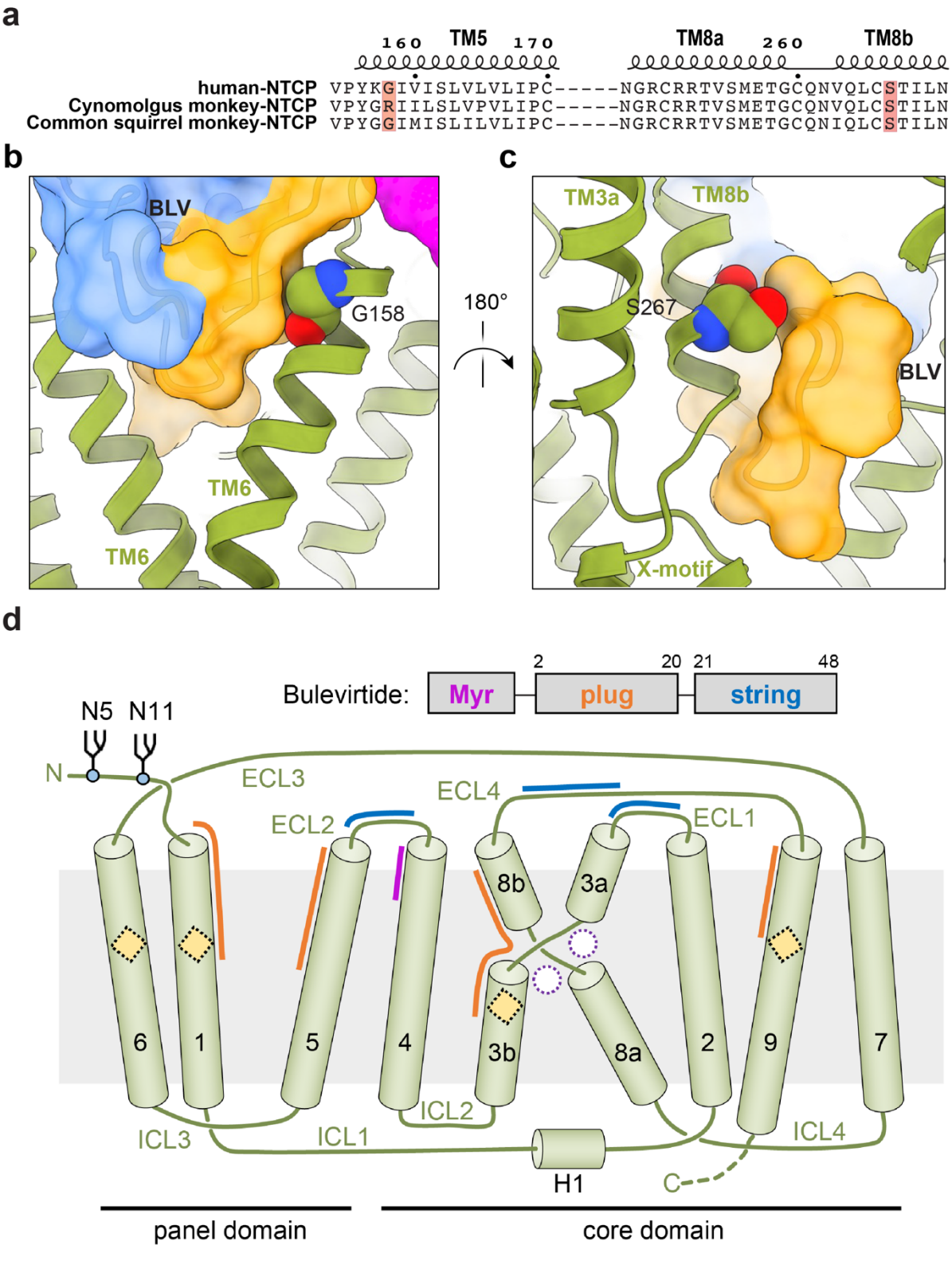

550
551

Figure Legends

Fig. 1: Schematic of human NTCP-mediated HBV infection

Bile salt uptake into hepatocytes is mediated by NTCP located in the basolateral membrane of hepatocytes. HBV particles interact with heparan sulfate proteoglycans (HSPGs) for low-affinity attachment. NTCP is recognized by HBV, initiating the entry of HBV particles into the hepatocytes via endocytosis, a process that may be facilitated by additional co-factors. The interaction between HBV and NTCP is mediated by the preS1 domain of the LHBs protein, which can be effectively inhibited by Bulevirtide, a preS1-derived peptide.

Fig. 2: Binding of preS1 and patient-derived SVPs as model systems to study HBV-NTCP interaction

a Fluorescence microscopy and **b** fluorescence detection of HEK-NTCP cells and non-NTCP expressing HEK293 cells after incubated with 200 nM fluorescent preS1-AX568 peptide (representing genotype D, GtD) in the presence and absence of sodium in the incubation buffer. Incubation of NBD-TC was used to demonstrate functional bile salt transport via NTCP and 250 μM TC were used as inhibitor of the preS1-peptide binding. Data in **b** presented means ± SD of quadruplicate determinations. *Significantly higher preS1-AX568 fluorescence compared to all other columns, §significantly different preS1 binding and $^{\#}$significant preS1 binding inhibition according to two-way ANOVA with Tukey's multiple comparison test, $p<0.001$. **c** Illustration of patient-derived HBV subviral particles. The hepatitis B virus surface proteins LHBs, MHBs, and SHBs are indicated that differ in amino-terminal additions (preS1, preS2) and N-glycosylation pattern within the S-domain. Determinants for infectivity of HBV are the antigenic loop (AGL) within the S-domain and the amino-terminal 75 amino acids of preS1 together with the covalently attached myristic acid at Gly2. The amino acids 9-15 within preS1 are highly conserved within primate HBV isolates and essential for HBV infectivity. **d** Representative silver-stained polyacrylamide gels of highly purified SVP preparations from two different patients: K826 HBV-GtA and ID1 HBV-GtD. Both preparations demonstrate clear banding of non- and N-glycosylated SHBs (p24/gp27 kDa), single- and double N-glycosylated

MHBs (gp33/ggp36 kDa), and non- and N-glycosylated preS1-containing LHBs (p39/gp42 kDa). Banding of non-reduced SHBs-dimers (48 kDa or 54 kDa, depending on glycosylation status) and human serum albumin (67 kDa) is indicated. Binding of recombinant wildtype or G158R mutant NTCP-eYFP nanodisc preparations to SVPs from **e** patient K826 (HBV GtA) and **f** patient ID1 (HBV GtD). NTCP-eYFP fluorescence was detected using a fluorescence microtiter plate reader at 485 nm excitation and 535 nm emission. Data presented means ± SD of triplicate determinations of background-subtracted relative fluorescence units (RFU) of representative experiments. *Significantly higher fluorescence intensity between SVP-coated wells incubated without or with NTCP-eYFP nanodisc preparations with $p<0.05$ according to one-way ANOVA with Dunnett's multiple comparison test.

Fig. 3: Cryo-EM structure and functional analysis of BLV-bound NTCP

a Normalized inhibition of TC transport (1 μM) into Flp-In T-Rex cells stably expressing NTCP at varying concentrations of BLV. Uptake of ^{3}H-TC was measured after 8 min, each data point indicates the mean of three independent replicates, and error bars represent the SD. **b** Size exclusion chromatography and SDS-PAGE analysis of purified human NTCP in a complex with BLV, Fab3, and a nanobody. **c** Cryo-EM density map (left) and structure in ribbon representation (right) of NTCP-BLV-Fab3-nanobody complex. The BLV peptide is colored into three sections: myristoylated glycine group (magenta), plug (orange), and string (blue).

Fig. 4: Molecular interaction between BLV and NTCP

a Surface representation of NTCP (green), with the bound BLV peptide: myristoylated glycine (magenta), residues T3-G20 (orange), and residues P21-G48 (blue). **b** 2D schematic of the full BLV sequence, coloring is the same as in **a**. **c** Sequence alignment of BLV and the preS1 peptides from ten genotypes of HBV. Blue shading indicates amino acids conservation between BLV and different HBV preS1 genotypes. Black asterisks denote residues of BLV that are exposed to the solvent and therefore do not interact with NTCP. **d-g** Interactions of

BLV with NTCP. NTCP is shown in green. The EM density for BLV is displayed as blue mesh. BLV residues are labelled black.

Fig. 5: Comparison of BLV-bound NTCP and substrate-bound NTCP

a-b Superposed BLV-bound NTCP (green) and substrate-bound NTCP (PDB ID: 7ZYI, gray) structures shown as ribbon. Two molecules of the substrate glycochenodeoxycholic acid (GCDC) are shown as gray sticks and the BLV peptide is colored as before. Close-up views show a clash between the substrate GCDC and TM6 of the BLV-bound NTCP structure (**a**), and a clash between GCDC substrates and the BLV peptide (**b**).

Fig. 6: NTCP species specificity against HBV infection

a Sequence alignment between human NTCP and NTCP from two different species of monkeys (Old World monkey-cynomolgus monkey and New World monkey-common squirrel monkey). Highlighted amino acids indicate the residues described in the text: the Gly/Arg variation at position 158, and the Ser267 that in humans resistant to HBV infection, is mutated into a phenylalanine residue. **b-c** A close-up view of residue Gly158 (sphere representation) and its proximity to BLV (yellow and blue transparent surface). **c** A close-up view of residue Ser267 (sphere representation) and its proximity to BLV (yellow and blue transparent surface). **d** Topology diagram of human NTCP. Sodium binding sites and regions interacting with bound substrates (both unoccupied in the NTCP-BLV structure) are indicated as empty circles and squares, respectively. ECH: extracellular helix, ICH: intracellular helix. The crossing motif (X-motif) is formed by TM helices 3 and 8. Glycosylation sites are shown and numbered. Colored arches indicate the regions of NTCP interacting with distinct regions of the BLV peptide.

References

1 Kabore, H. J. *et al.* Progress Toward Hepatitis B Control and Elimination of Mother-to-Child Transmission of Hepatitis B Virus - World Health Organization African Region, 2016-2021. *MMWR Morb Mortal Wkly Rep* **72**, 782-787 (2023). https://doi.org/10.15585/mmwr.mm7229a2

2 Leoni, S., Casabianca, A., Biagioni, B. & Serio, I. Viral hepatitis: Innovations and expectations. *World J Gastroenterol* **28**, 517-531 (2022). https://doi.org/10.3748/wjg.v28.i5.517

3 Zhang, Y. Y. & Hu, K. Q. Rethinking the pathogenesis of hepatitis B virus (HBV) infection. *J Med Virol* **87**, 1989-1999 (2015). https://doi.org/10.1002/jmv.24270

4 Rizzetto, M. Hepatitis D Virus: Introduction and Epidemiology. *Cold Spring Harb Perspect Med* **5**, a021576 (2015). https://doi.org/10.1101/cshperspect.a021576

5 Caviglia, G. P., Ciancio, A. & Rizzetto, M. A Review of HDV Infection. *Viruses* **14**, 1749 (2022). https://doi.org/10.3390/v14081749

6 Asselah, T. & Rizzetto, M. Hepatitis D Virus Infection. *N Engl J Med* **389**, 58-70 (2023). https://doi.org/10.1056/NEJMra2212151

7 Yan, H. & Li, W. Sodium taurocholate cotransporting polypeptide acts as a receptor for hepatitis B and D virus. *Dig Dis* **33**, 388-396 (2015). https://doi.org/10.1159/000371692

8 Yan, H. *et al.* Sodium taurocholate cotransporting polypeptide is a functional receptor for human hepatitis B and D virus. *Elife* **1**, e00049 (2012). https://doi.org/10.7554/eLife.00049

9 Leistner, C. M., Gruen-Bernhard, S. & Glebe, D. Role of glycosaminoglycans for binding and infection of hepatitis B virus. *Cell Microbiol* **10**, 122-133 (2008). https://doi.org/10.1111/j.1462-5822.2007.01023.x

10 Herrscher, C., Roingeard, P. & Blanchard, E. Hepatitis B Virus Entry into Cells. *Cells* **9**, 1486 (2020). https://doi.org/10.3390/cells9061486

11 Schulze, A., Gripon, P. & Urban, S. Hepatitis B virus infection initiates with a large surface protein-dependent binding to heparan sulfate proteoglycans. *Hepatology* **46**, 1759-1768 (2007). https://doi.org/10.1002/hep.21896

12 Sureau, C. & Salisse, J. A conformational heparan sulfate binding site essential to infectivity overlaps with the conserved hepatitis B virus a-determinant. *Hepatology* **57**, 985-994 (2013). https://doi.org/10.1002/hep.26125

13 König, A. *et al.* Kinetics of the bile acid transporter and hepatitis B virus receptor Na+/taurocholate cotransporting polypeptide (NTCP) in hepatocytes. *J Hepatol* **61**, 867-875 (2014). https://doi.org/10.1016/j.jhep.2014.05.018

14 Ni, Y. *et al.* Hepatitis B and D viruses exploit sodium taurocholate co-transporting polypeptide for species-specific entry into hepatocytes. *Gastroenterology* **146**, 1070-1083 (2014). https://doi.org/10.1053/j.gastro.2013.12.024

15 Durník, R., Šindlerová, L., Babica, P. & Jurček, O. Bile Acids Transporters of Enterohepatic Circulation for Targeted Drug Delivery. *Molecules* **27**, 2961 (2022). https://doi.org/10.3390/molecules27092961

16 Roberts, M. S., Magnusson, B. M., Burczynski, F. J. & Weiss, M. Enterohepatic circulation: physiological, pharmacokinetic and clinical implications. *Clin Pharmacokinet* **41**, 751-790 (2002). https://doi.org/10.2165/00003088-200241100-00005

17 Geyer, J., Wilke, T. & Petzinger, E. The solute carrier family SLC10: more than a family of bile acid transporters regarding function and phylogenetic relationships. *Naunyn Schmiedebergs Arch Pharmacol* **372**, 413-431 (2006). https://doi.org/10.1007/s00210-006-0043-8

18 Meier, P. J. & Stieger, B. Bile salt transporters. *Annu Rev Physiol* **64**, 635-661 (2002). https://doi.org/10.1146/annurev.physiol.64.082201.100300

19 Trauner, M. & Boyer, J. L. Bile salt transporters: molecular characterization, function, and regulation. *Physiol Rev* **83**, 633-671 (2003). https://doi.org/10.1152/physrev.00027.2002

20 Goutam, K., Ielasi, F. S., Pardon, E., Steyaert, J. & Reyes, N. Structural basis of sodium-dependent bile salt uptake into the liver. *Nature* **606**, 1015-1020 (2022). https://doi.org/10.1038/s41586-022-04723-z

21 Asami, J. *et al.* Structure of the bile acid transporter and HBV receptor NTCP. *Nature* **606**, 1021-1026 (2022). https://doi.org/10.1038/s41586-022-04845-4

22 Park, J. H. *et al.* Structural insights into the HBV receptor and bile acid transporter NTCP. *Nature* **606**, 1027-1031 (2022). https://doi.org/10.1038/s41586-022-04857-0

23 Liu, H. *et al.* Structure of human NTCP reveals the basis of recognition and sodium-driven transport of bile salts into the liver. *Cell Res* **32**, 773-776 (2022). https://doi.org/10.1038/s41422-022-00680-4

24 Seitz, S., Habjanič, J., Schütz, A. K. & Bartenschlager, R. The Hepatitis B Virus Envelope Proteins: Molecular Gymnastics Throughout the Viral Life Cycle. *Annu Rev Virol* **7**, 263-288 (2020). https://doi.org/10.1146/annurev-virology-092818-015508

25 Bruss, V. & Ganem, D. The role of envelope proteins in hepatitis B virus assembly. *Proc Natl Acad Sci U S A* **88**, 1059-1063 (1991). https://doi.org/10.1073/pnas.88.3.1059

26 Glebe, D. & Urban, S. Viral and cellular determinants involved in hepadnaviral entry. *World J Gastroenterol* **13**, 22-38 (2007). https://doi.org/10.3748/wjg.v13.i1.22

27 Glebe, D. & Bremer, C. M. The molecular virology of hepatitis B virus. *Semin Liver Dis* **33**, 103-112 (2013). https://doi.org/10.1055/s-0033-1345717

28 Glebe, D. *et al.* Mapping of the hepatitis B virus attachment site by use of infection-inhibiting preS1 lipopeptides and tupaia hepatocytes. *Gastroenterology* **129**, 234-245 (2005). https://doi.org/10.1053/j.gastro.2005.03.090

29 Meier, A., Mehrle, S., Weiss, T. S., Mier, W. & Urban, S. Myristoylated PreS1-domain of the hepatitis B virus L-protein mediates specific binding to differentiated hepatocytes. *Hepatology* **58**, 31-42 (2013). https://doi.org/10.1002/hep.26181

30 Sureau, C., Guerra, B. & Lanford, R. E. Role of the large hepatitis B virus envelope protein in infectivity of the hepatitis delta virion. *J Virol* **67**, 366-372 (1993). https://doi.org/10.1128/jvi.67.1.366-372.1993

31 Le Seyec, J., Chouteau, P., Cannie, I., Guguen-Guillouzo, C. & Gripon, P. Infection process of the hepatitis B virus depends on the presence of a defined sequence in the pre-S1 domain. *J Virol* **73**, 2052-2057 (1999). https://doi.org/10.1128/jvi.73.3.2052-2057.1999

32 Schulze, A., Schieck, A., Ni, Y., Mier, W. & Urban, S. Fine mapping of pre-S sequence requirements for hepatitis B virus large envelope protein-mediated receptor interaction. *J Virol* **84**, 1989-2000 (2010). https://doi.org/10.1128/jvi.01902-09

33 Yan, H. *et al.* Molecular determinants of hepatitis B and D virus entry restriction in mouse sodium taurocholate cotransporting polypeptide. *J Virol* **87**, 7977-7991 (2013). https://doi.org/10.1128/jvi.03540-12

34 Palatini, M. *et al.* IFITM3 Interacts with the HBV/HDV Receptor NTCP and Modulates Virus Entry and Infection. *Viruses* **14**, 727 (2022). https://doi.org/10.3390/v14040727

35 Iwamoto, M. *et al.* Epidermal growth factor receptor is a host-entry cofactor triggering hepatitis B virus internalization. *Proc Natl Acad Sci U S A* **116**, 8487-8492 (2019). https://doi.org/10.1073/pnas.1811064116

36 Gerlich, W. H. *et al.* Occult hepatitis B virus infection: detection and significance. *Dig Dis* **28**, 116-125 (2010). https://doi.org/10.1159/000282074

37 Jiang, B. & Hildt, E. Intracellular Trafficking of HBV Particles. *Cells* **9**, 2023 (2020). https://doi.org/10.3390/cells9092023

38 Cao, J. *et al.* Cryo-EM structure of native spherical subviral particles isolated from HBV carriers. *Virus Res* **259**, 90-96 (2019). https://doi.org/10.1016/j.virusres.2018.10.015

39 Chai, N. *et al.* Properties of subviral particles of hepatitis B virus. *J Virol* **82**, 7812-7817 (2008). https://doi.org/10.1128/jvi.00561-08

40 Gripon, P., Cannie, I. & Urban, S. Efficient inhibition of hepatitis B virus infection by acylated peptides derived from the large viral surface protein. *J Virol* **79**, 1613-1622 (2005). https://doi.org/10.1128/jvi.79.3.1613-1622.2005

41 Schieck, A. *et al.* Hepatitis B virus hepatotropism is mediated by specific receptor recognition in the liver and not restricted to susceptible hosts. *Hepatology* **58**, 43-53 (2013). https://doi.org/10.1002/hep.26211

42 Blank, A. *et al.* First-in-human application of the novel hepatitis B and hepatitis D virus entry inhibitor myrcludex B. *J Hepatol* **65**, 483-489 (2016). https://doi.org/10.1016/j.jhep.2016.04.013

43 Cheng, D., Han, B., Zhang, W. & Wu, W. Clinical effects of NTCP-inhibitor myrcludex B. *J Viral Hepat* **28**, 852-858 (2021). https://doi.org/10.1111/jvh.13490

44 Loglio, A. *et al.* Excellent safety and effectiveness of high-dose myrcludex-B monotherapy administered for 48 weeks in HDV-related compensated cirrhosis: A case report of 3 patients. *J Hepatol* **71**, 834-839 (2019). https://doi.org/10.1016/j.jhep.2019.07.003

45 Donkers, J. M., Appelman, M. D. & van de Graaf, S. F. J. Mechanistic insights into the inhibition of NTCP by myrcludex B. *JHEP Rep* **1**, 278-285 (2019). https://doi.org/10.1016/j.jhepr.2019.07.006

46 Hagenbuch, B. & Meier, P. J. Sinusoidal (basolateral) bile salt uptake systems of hepatocytes. *Semin Liver Dis* **16**, 129-136 (1996). https://doi.org/10.1055/s-2007-1007226

47 Nkongolo, S. *et al.* Cyclosporin A inhibits hepatitis B and hepatitis D virus entry by cyclophilin-independent interference with the NTCP receptor. *J Hepatol* **60**, 723-731 (2014). https://doi.org/10.1016/j.jhep.2013.11.022

48 Miller, K. R. *et al.* T cell receptor-like recognition of tumor in vivo by synthetic antibody fragment. *PLoS One* **7**, e43746 (2012). https://doi.org/10.1371/journal.pone.0043746

762 49 Ereño-Orbea, J. *et al.* Structural Basis of Enhanced Crystallizability Induced by a
763 Molecular Chaperone for Antibody Antigen-Binding Fragments. *J Mol Biol* **430**, 322-
764 336 (2018). https://doi.org/10.1016/j.jmb.2017.12.010
765 50 Bruss, V., Hagelstein, J., Gerhardt, E. & Galle, P. R. Myristylation of the large surface
766 protein is required for hepatitis B virus in vitro infectivity. *Virology* **218**, 396-399
767 (1996). https://doi.org/10.1006/viro.1996.0209
768 51 Gripon, P., Le Seyec, J., Rumin, S. & Guguen-Guillouzo, C. Myristylation of the
769 hepatitis B virus large surface protein is essential for viral infectivity. *Virology* **213**,
770 292-299 (1995). https://doi.org/10.1006/viro.1995.0002
771 52 Yan, H. *et al.* Viral Entry of Hepatitis B and D Viruses and Bile Salts Transportation
772 Share Common Molecular Determinants on Sodium Taurocholate Cotransporting
773 Polypeptide. *Journal of Virology* **88**, 3273-3284 (2014).
774 https://doi.org/10.1128/jvi.03478-13
775 53 Wedemeyer, H. *et al.* A Phase 3, Randomized Trial of Bulevirtide in Chronic Hepatitis
776 D. *N Engl J Med* **389**, 22-32 (2023). https://doi.org/10.1056/NEJMoa2213429
777 54 Müller, S. F., König, A., Döring, B., Glebe, D. & Geyer, J. Characterisation of the
778 hepatitis B virus cross-species transmission pattern via Na+/taurocholate co-
779 transporting polypeptides from 11 New World and Old World primate species. *PLoS*
780 *One* **13**, e0199200 (2018). https://doi.org/10.1371/journal.pone.0199200
781 55 Takeuchi, J. S. *et al.* A Single Adaptive Mutation in Sodium Taurocholate
782 Cotransporting Polypeptide Induced by Hepadnaviruses Determines Virus Species
783 Specificity. *J Virol* **93**, e01432-01418 (2019). https://doi.org/10.1128/jvi.01432-18
784 56 Shofa, M., Ohkawa, A., Kaneko, Y. & Saito, A. Conserved use of the sodium/bile acid
785 cotransporter (NTCP) as an entry receptor by hepatitis B virus and domestic cat
786 hepadnavirus. *Antiviral Res* **217**, 105695 (2023).
787 https://doi.org/10.1016/j.antiviral.2023.105695
788 57 Pan, W. *et al.* Genetic polymorphisms in Na+-taurocholate co-transporting
789 polypeptide (NTCP) and ileal apical sodium-dependent bile acid transporter (ASBT)

and ethnic comparisons of functional variants of NTCP among Asian populations. *Xenobiotica* **41**, 501-510 (2011). https://doi.org/10.3109/00498254.2011.555567

58 Ruggiero, M. J. *et al.* A clinically relevant polymorphism in the Na(+)/taurocholate cotransporting polypeptide (NTCP) occurs at a rheostat position. *J Biol Chem* **296**, 100047 (2021). https://doi.org/10.1074/jbc.RA120.014889

59 Peng, L. *et al.* The p.Ser267Phe variant in SLC10A1 is associated with resistance to chronic hepatitis B. *Hepatology* **61**, 1251-1260 (2015). https://doi.org/10.1002/hep.27608

60 Binh, M. T. *et al.* NTCP S267F variant associates with decreased susceptibility to HBV and HDV infection and decelerated progression of related liver diseases. *Int J Infect Dis* **80**, 147-152 (2019). https://doi.org/10.1016/j.ijid.2019.01.038

61 Asami, J. *et al.* Structural basis of hepatitis B virus receptor binding. *Nat Struct Mol Biol* (2024). https://doi.org/10.1038/s41594-023-01191-5

62 Zakrzewicz, D. *et al.* Tyrosine 146 of the Human Na(+)/Taurocholate Cotransporting Polypeptide (NTCP) Is Essential for Its Hepatitis B Virus (HBV) Receptor Function and HBV Entry into Hepatocytes. *Viruses* **14**, 1259 (2022). https://doi.org/10.3390/v14061259

63 Petzinger, E., Wickboldt, A., Pagels, P., Starke, D. & Kramer, W. Hepatobiliary transport of bile acid amino acid, bile acid peptide, and bile acid oligonucleotide conjugates in rats. *Hepatology* **30**, 1257-1268 (1999). https://doi.org/10.1002/hep.510300529

64 Paduch, M. *et al.* Generating conformation-specific synthetic antibodies to trap proteins in selected functional states. *Methods* **60**, 3-14 (2013). https://doi.org/10.1016/j.ymeth.2012.12.010

65 Hornsby, M. *et al.* A High Through-put Platform for Recombinant Antibodies to Folded Proteins. *Mol Cell Proteomics* **14**, 2833-2847 (2015). https://doi.org/10.1074/mcp.O115.052209

66 Bloch, J. S. *et al.* Development of a universal nanobody-binding Fab module for fiducial-assisted cryo-EM studies of membrane proteins. *Proc Natl Acad Sci U S A* **118**, e2115435118 (2021). https://doi.org/10.1073/pnas.2115435118

67 Emsley, P., Lohkamp, B., Scott, W. G. & Cowtan, K. Features and development of Coot. *Acta Crystallogr D Biol Crystallogr* **66**, 486-501 (2010). https://doi.org/10.1107/s0907444910007493

68 Liebschner, D. *et al.* Macromolecular structure determination using X-rays, neutrons and electrons: recent developments in Phenix. *Acta Crystallogr D Struct Biol* **75**, 861-877 (2019). https://doi.org/10.1107/s2059798319011471

69 Williams, C. J. *et al.* MolProbity: More and better reference data for improved all-atom structure validation. *Protein Sci* **27**, 293-315 (2018). https://doi.org/10.1002/pro.3330

70 Pettersen, E. F. *et al.* UCSF Chimera--a visualization system for exploratory research and analysis. *J Comput Chem* **25**, 1605-1612 (2004). https://doi.org/10.1002/jcc.20084

71 Pettersen, E. F. *et al.* UCSF ChimeraX: Structure visualization for researchers, educators, and developers. *Protein Sci* **30**, 70-82 (2021). https://doi.org/10.1002/pro.3943